# ARTICLE IN PRESS

Journal of the European Ceramic Society xxx (xxxx) xxx-xxx



Contents lists available at ScienceDirect

# Journal of the European Ceramic Society

journal homepage: www.elsevier.com/locate/jeurceramsoc



## Original Article

# Single step densification of high permittivity BaTiO<sub>3</sub> ceramics at 300 °C

Kosuke Tsuji<sup>a,b,\*</sup>, Arnaud Ndayishimiye<sup>a,b</sup>, Sarah Lowum<sup>b</sup>, Richard Floyd<sup>b</sup>, Ke Wang<sup>a</sup>, Maxwell Wetherington<sup>a</sup>, Jon-Paul Maria<sup>b</sup>, Clive A. Randall<sup>a,b</sup>

#### ARTICLE INFO

Keywords:
Cold sintering process
Barium titanate
Ferroelectric size effect
Low temperature sintering
Ceramic capacitor

#### ABSTRACT

Dense nanocrystalline BaTiO $_3$  ceramics are prepared in a single step by the Cold Sintering Process at 300 °C, under a uniaxial pressure of 520 MPa for 12 h using a molten hydroxide flux. Transmission electron microscopy reveals a dense microstructure with sharp grain boundaries. The average grain sizes are 75–150 nm depending on the flux amount. The dielectric permittivity is 700–1800 at room temperature at 10<sup>6</sup> Hz, with a dielectric loss, tan  $\delta \sim 0.04$ . The difference in permittivity and phase transition behavior are explained in terms of the intrinsic size effect of the BaTiO $_3$ . The nanocrystalline BaTiO $_3$  ceramics still shows a macroscopic ferroelectric switching via a hysteresis loop. This work demonstrates that cold-sintering process could enable the densification of ferroelectric oxides in a single step. Futhermore, comparable dielectric properties to reported values for nanocrystalline grains are obtained, but at this time, with the lowest processing temperatures ever used.

### 1. Introduction

BaTiO<sub>3</sub> is one of the most important electroceramic materials. It is the basic compound that is doped to produce high permittivity dielectric materials used in multilayer capacitor components. These components are extremely useful in the control of modern electronic circuit charge supply. Over three trillion multilayer ceramic capacitors are used each year. Of those, 90 % of the components are manufactured with inner electrodes of nickel that are cofired with a formulated  $BaTiO_3$  at sintering temperature of  $\sim 1250$  °C and an atmosphere of  $pO_2 \, \sim \, 10^{-12}$  atms with a gas mixture of  $N_2\text{-H}_2\text{-H}_2\text{O}.$  Cold Sintering Process (CSP) is a relative new concept but has been applied to a number of materials, many of which could also be densified to extremely high densities and properties at temperatures below 300 °C [1–4]. In some materials, including perovskite-based ferroelectrics such as BaTiO3 [5], Pb(Zr,Ti)O3 [6], and SrTiO3 [7], sintering was accomplished at low temperature conditions; however, the dielectric properties, such as the permittivity and remanent polarization, are limited without a secondary thermal treatment. In the case of the earlier studies on BaTiO3, it was the use of a transient liquid with stoichiometric adjustments to limit incongruent dissolution. This added to the densification but still leads to glassy phases in the grain boundaries that have a major limitation to the dielectric properties of these ferroelectric materials. However, on heat treatments ranging from 700 °C to 900 °C, these grain boundaries equilibrate, and the glassy phase is incorporated

into crystalline material. The metastable glass in the  $BaTiO_3$  microstructure is associated with a  $BaCO_3$  phase. This phase has to decompose to allow the complete densification of the microstructure and the glassy interface dominants the dielectric properties limiting performance without this secondary heat treatment. Alkali metal hydroxide fluxes have been employed as "high-temperature solutions" to aid synthesizing new oxides and grow crystals of known compositions and structures [8]. The NaOH-KOH mixture have a eutectic point of 170 °C and it has been used for synthesizing a variety of complex oxides at low temperatures [9–13]. The objective of this study is to utilize hydroxide additives to aid the cold sintering of  $BaTiO_3$  and avoid the second heat treatments following the preliminary work in some binary oxides [14]. The microstructure and comparisons of the dielectric properties will be made relative to previous reports on high quality  $BaTiO_3$  materials fabricated at high temperatures with submicron grain sizes.

## 2. Experimental

#### 2.1. Materials preparation

BaTiO $_3$  nanopowder (Toda BT-020, average particle size: 20 nm, BET surface area = 30.2 m $^2$  g $^{-1}$ ) was used in this study. The BET surface area was determined by N $_2$  gas molecule adsorption (ASAP 2020, Micromeritics). The as-received powder (0.80 g) was mixed with 4 and 6 wt% of mixture of NaOH (Fisher Scientific, > 98 %) and KOH

https://doi.org/10.1016/j.jeurceramsoc.2019.12.022

Received 26 October 2019; Received in revised form 9 December 2019; Accepted 9 December 2019 0955-2219/ © 2019 Elsevier Ltd. All rights reserved.

<sup>&</sup>lt;sup>a</sup> Materials Research Institute, The Pennsylvania State University, University Park, Pennsylvania, 16802, USA

<sup>&</sup>lt;sup>b</sup> Department of Materials Science and Engineering, The Pennsylvania State University, University Park, PA, 16802, USA

<sup>\*</sup> Corresponding author at: Materials Research Institute, The Pennsylvania State University, University Park, Pennsylvania, 16802, USA. *E-mail address*: tuk152@psu.edu (K. Tsuji).

K. Tsuji, et al.

(Fisher Scientific, > 85 %) in 50:50 M ratio. After being thoroughly grounded, the powders were uniaxially pressed at 520 MPa and at heated to 300 °C with a heater band and plates on the top and bottom. The average ramp rate was 19.5 °C/min and hold for 12 h. Detail experimental setup is described elsewhere [15,16]. The densities of the cold-sintered pellets were geometrically measured based on the mass and volume of the pellets.

#### 2.2. Characterization

Phase purity was investigated by the X-ray diffraction (XRD, Empyrean, PANalytical) with a scan rate of  $0.067^{\circ}/s$  using Cu K $\alpha$ . Raman spectra were measured with Raman microscope (Horiba, Vlabinir, 532 nm). The microstructures were observed by Field Emission Scanning Emission Microscopy (Leo 1550, Carl Zeiss, Inc., Jena, Germany) for fracture surfaces. The transmission electron microscope (TEM) samples were prepared by the Focused Ion Beam (FEI Helios NanoLab 660 FIB) system and the TEM analysis was done by FEI Talos F200  $\times$ . Average grain size was calculated from the polished surface using the line intercept method [17]. The 80 nm of Pt electrodes were deposited by sputtering (Q150R Plus, Quorum) for the electrical measurement. Dielectric properties were investigated with HP 4284A precision LCR meter. The polarization-field (*P-E*) hysteresis loop of the BT-75 nm was measured using a Sawyer-Tower circuit with a Trek Model 30/20 high voltage amplifier system (Trek, Inc., Lockport, NY).

#### 3. Results and discussion

Fig. 1(a,d) and (b,c) show microstructures of the two cold-sintered specimens, at low and high magnification of transmission electron microscopy (TEM). It is clearly seen that two specimens possess highly dense microstructures with homogeneous grain sizes. The average grain sizes were 150 nm and 75 nm for 4 and 6 wt% of hydroxide fluxes. Hereafter, we name these specimens as BT-150 nm and BT-75 nm respectively. The obtained bulk densities were 5.55 and 5.80 g cm $^{-3}$  for BT-150 nm and BT-75 nm, respectively. These values correspond to 92 and 96 % of the theoretical density of the pure BaTiO $_3$  (6.03 g cm $^{-3}$ ). As the real density of the pellet should be different from the theoretical value because of the presence of the hydroxides, real densities of the specimens were determined by He pycnometry to be 5.67 and 5.83 g cm $^{-3}$ , for BT-150 nm and BT-75 nm. Relative densities to the real densities were therefore 98 % and 99 %. Besides that, BET surface area

substantially decreased from  $30.2~\text{m}^2~\text{g}^{\text{-1}}$  of the initial powder to 0.3~and0.4 m<sup>2</sup> g<sup>-1</sup> after CSP for BT-150 nm and BT-75 nm, respectively. Significant surface area reduction is another indication of high degree of densification of BaTiO3 at 300 °C, which is much lower than typical sintering temperature. As reported for nanoparticles synthesis, molten hydroxides are very useful fluxes for low temperature BaTiO<sub>3</sub> synthesis [13]. It is speculated that the flux plays the role in densification as a high temperature solvent that induced the pressure-solution creep and provided thermodynamically stable conditions for BaTiO<sub>3</sub> ceramics in the Cold-Sintering conditions applied [16,18-21]. It is important to note that experimental condition used in this work aren't fully optimized. BaTiO<sub>3</sub> could be densified within 3 h under similar conditions (Fig. S1). A relatively long sintering time was used in this study to minimized porosity. Scanning TEM mode reveals that some internal defect inclusions exist in grains of BaTiO<sub>3</sub> in Fig. 1(c,g). These are often observed in the sintered BaTiO3 ceramics when low temperature hydrothermally- or solvochemically- synthesized BaTiO3 powders are used, due to the presence of hydroxyl group [22-24]. As FTIR and TGA showed the presence of hydroxyl group in the initial nanopowder (Fig. S2) and the final microstructure is very similar to the reported literature in the conventionally sintered BaTiO3 ceramics with hydrothermallyderived starting powder [22], it should be reasonable to conclude that the internal defects in Fig. 1(c,g) are not a specific consequence of CSP. The observed dense shell region in Fig. 1(c) may grow during CSP. Some minor pores at core region may affect some properties under high voltage [25]. The CSP for BaTiO3 using a powder derived in the solidstate route is under investigation. Besides these minor defects and closed pores, specimens show equiaxed grains with equilibrated triple points which are a feature of the final stage of the sintering. Ferroelectric-ferroelastic non-180° domain structures are not observed in the grains. Fig. 1(d) and (h) revealed the well-crystallized grain boundaries after the cold sintering. The clean grain boundary formation without glassy phase was previously not observed until a second heat treatment was applied after cold sintering to temperatures 800 – 900 °C [5]. An elemental analysis with energy dispersion spectroscopy in the TEM indicates there are no detectable alkaline ions in the grains or grain boundaries (Fig. S3). It should be noted that the presence of the remaining hydroxides islands can be observed on a fracture surface by Scanning Electron Microscopy, (Supplementary Fig. S4). The majority of the hydroxide flux is believed to exist as segregated precipitates with relatively large scale (> 1 µm), not in grains. The absence of NaOH-KOH in the TEM-EDS is probably because the hydroxides were

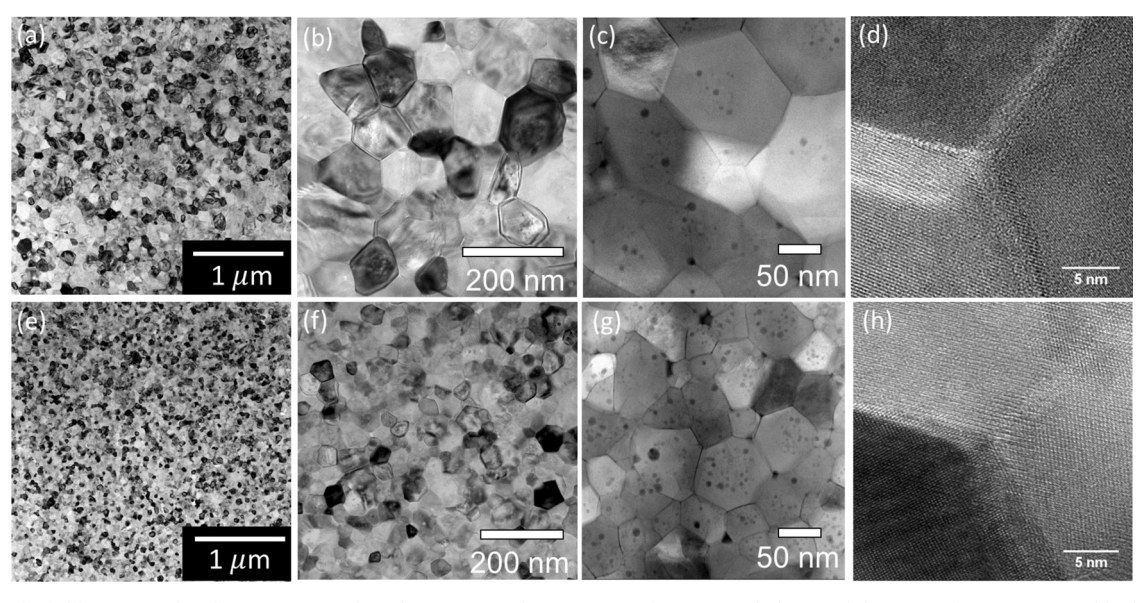


Fig. 1. TEM bright field micrographs of BT-150 nm (a–d) and BT-75 nm(e–h). Overview of grain morphology with low magnification (a,e) and high magnification (b,f). Grain morphology with STEM mode (c,g) Grain boundary microstructures (d,h).

K. Tsuji, et al.

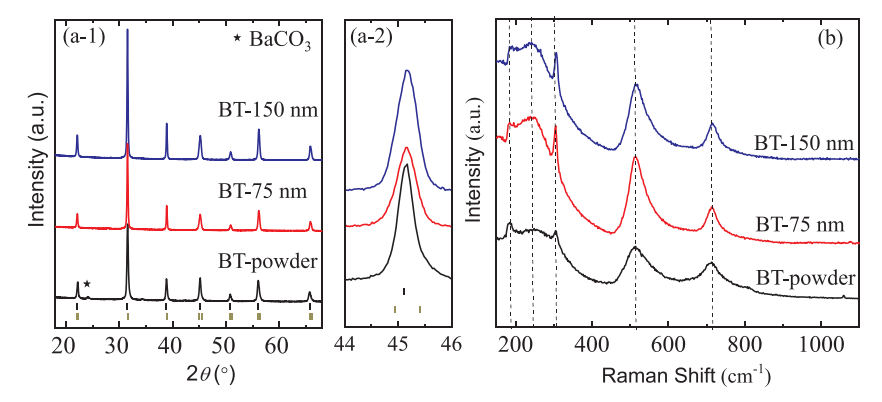


Fig. 2. XRD patterns (a), and Raman spectrum (b), of initial powder (BT-powder) and cold sintered BaTiO<sub>3</sub> ceramics. (a-2) shows expanded view of 200 reflection. Peak position for cubic (upper: PDF# 04-013-5284) and tetragonal (lower: PDF#04-015-6089) are identified with the bars.

preferentially removed during the sample preparation for TEM.

Fig. 2(a) shows X-ray diffraction of the initial powder (BT-powder) and sintered specimens, respectively. It appears all the specimens possess a perovskite phase as a major phase. The small amount of the impurity phase (BaCO<sub>3</sub>) is only seen in the initial powder and disappeared after CSP. The molten hydroxide may have provided the thermodynamically stable conditions that preferred the perovskite formation over the BaCO3, as already observed under hydrothermal conditions [26,27]. No obvious peaks from hydroxide phases are found in X-ray diffraction pattern, probably due to their small proportion and/ or their low crystallinity. Fig. 2(a-2) shows a peak from 200 reflection. The single peak of 200 reflection indicates that all the specimens are the pseudo-cubic structure. The peak shape is nearly same in the form of the ceramic pellet and grinded ceramic (Fig. S5). It should be addressed that the XRD is not able to sufficiently resolve the spontaneous distorted structure in the size of 100 nm scale. Therefore, Raman Spectroscopy was performed, as it has already been successfully used to reveal the local structure of BaTiO<sub>3</sub> [23,28].

Fig. 2(b) shows Raman spectra of BT-75 nm, 150 nm and BT-powder ( $\sim$ 20 nm) at room temperature. While cubic structure ( $Pm\bar{3}$  m) is not Raman active, the tetragonal crystal symmetry (P4mm) should represent  $3A_1 + B_1 + 4E$  of the Raman active mode. The spectra in the sintered ceramics shows 5 peaks at 187  $[A_1(LO)]$ , 260  $[A_1(TO)]$ , 306  $[B_1, E(TO + LO)], 515 [A_1, E(TO)]$ and 715  $[A_1, E(LO)]$ cm<sup>-1</sup> respectively. More than one mode is assigned because peak position of A and E mode is close. A complete peak assignment can be found elsewhere [29]. The spectra resemble the earlier work of orthorhombic or tetragonal BaTiO<sub>3</sub> [30-32]. Phase identification of orthorhombic and tetragonal phase is not discussed in this study as Raman spectra of those phase in the nanocrystalline BaTiO<sub>3</sub> are alike and difficult to differentiate due to the diffused phase transition at the nanograin size [30]. As many authors proposed [28,30,33,34], the co-existence of these phases is possible. The presence of those Raman band suggests that cold-sintered specimens should have at least local the tetragonal and/or orthorhombic structure and therefore ferroelectric properties are ex-

Fig. 3(a) shows the temperature dependence of dielectric properties. The room temperature permittivity is 1830 and 690 for BT-150 nm and BT-75 nm, respectively. The high permittivities and distinct Ferroelectric-Paraelectric phase transition indicate the dielectric properties are comparable to those sintered at high temperature. As Fig. 3(a) shows, smaller grain size (BT-75 nm) shows a lower dielectric permittivity at measured temperature range. The difference in the dielectric permittivity is explained in terms of the intrinsic size effect below 100 nm. Arlt et al. and others explained that the maximum of the permittivity appears around grain sizes of 0.8–1  $\mu$ m due to the 90° domain extrinsic contribution. Below this size, the permittivity constantly decreases due to the decrease of the tetragonality [33,35]. Fundamentally,

grain size effects can be observed in BaTiO3 with control of the grain sizes. The most comprehensive study on BaTiO3 was demonstrated with the use of spark plasma sintering (SPS) controlled grain sized materials from the late Nanni group [31,36,37]. In addition, there is also very good size effect data from others with hot pressing and crystallization of BaTiO<sub>3</sub> [28,33,38]. Here we contrast the cold sintering data with many of the earlier size effect reports. The permittivities in the present work follow the trend in a number of the studies on the grain size dependence (Fig. 3(b)) [33,36,38-43]. A slight difference from the trend in the reported values may be due to the remaining hydroxides and/or intragranular pores but the velues in this study are still comparable to those in SPS study. The dielectric anomaly appeared around 120 °C that is associated with the tetragonal -cubic displacive phase transition. The corresponding inverse permittivity shows a linear relationship with the temperature (Fig. 3(c)). It is clear that the phase transitions obey the Curie-Weiss law  $(1/\varepsilon_r = (T - \theta_C) / C' 1/\varepsilon_r = (T - \theta_C)/C' : \theta_C$  is Curie-Weiss temperature and C' is constant). The parameters obtained are listed in Table 1. The Curie-Weiss constant, C' for BT-150 nm and BT-75 nm, are reasonable values for the reported values in the BaTiO<sub>3</sub> [44,45]. A number of the theoretical and experimental studies showed that the transition temperatures of  $T_{O-T}$  and  $T_{C}$  have a grain (crystalline size) dependence [33,36,38-42,46,47]. Namely, the phase transition becomes the diffused character and then a slight increase of  $T_{O-T}$  and decrease of  $T_C$  are expected. As shown in Fig. 3(d), the  $T_{C-T}$  and  $T_C$  in this study are good agreement with the reported intrinsic size dependences. Finally, the values of  $\theta_{\rm C}$  in the present study are also in the range of the reported values of BaTiO3 sintered by SPS and Hot-Press Sintering methods. Overall, dielectric properties and phase transition behaviors of the cold-sintered BaTiO<sub>3</sub> nanocrystalline ceramics are well-explained by the size effect. It is noteworthy that these cold sintered BaTiO3 dielectrics are densified under the lowest sintering temperatures with high permittivity values, earlier it was thought that only high permittivities could be obtained only with higher thermal treatments [48].

Fig. 4 shows the polarization-field (P-E) hysteresis loop of the BT-75 nm. A hysteresis loop indicates the ferroelectric switching with a remanent polarization,  $P_{\rm r}$ , of 15.0  $\mu$ C cm<sup>-2</sup> and coercive,  $E_{\rm C}$ , of 18.6 kV cm<sup>-1</sup>. There are very few reports for the "macroscopic" ferroelectric switching behavior in the BaTiO<sub>3</sub> nanocrystalline ceramics [37,38,49,50]. The bulk P-E hysteresis were often the nearly linear so that evidence of the ferroelectric switching in the nano-grain ceramics has been limited in the "local" phenomena by the piezoresponse force microscopy [49,50]. The reason why the BT-75 nm in the present work can still show macroscopic ferroelectric switching behavior is not clear. It could be owing to sharp grain boundary microstructures that minimize the dilution of ferroelectric properties resulting from the nonferroelectric grain boundary layers, or simply due to relatively larger grains compared to 20 – 50 nm in the ref. [38,49,50]. In contrast to the

K. Tsuji, et al.

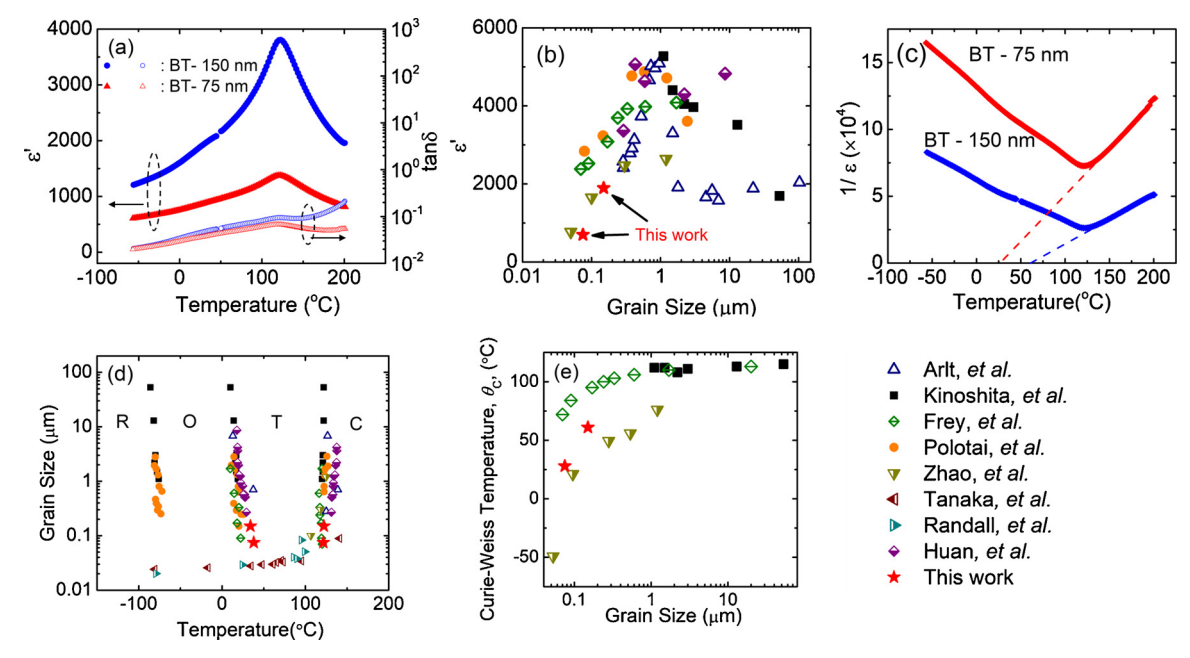


Fig. 3. (a) Temperature dependence of dielectric properties of cold sintered BaTiO<sub>3</sub> ceramics at 10<sup>6</sup> Hz. (b) Grain size effect on the relative permittivity for bulk BaTiO<sub>3</sub> ceramics. (c) Curie – Weiss plot. (d) Grain size dependence of phase transition temperature of the cold-sintered BaTiO<sub>3</sub>. R, O, T and C indicate Rhombohedral, Orthorhombic, Tetragonal, and Cubic crystal structure, (e) Grain size dependence of Curie-Weiss temperatures. Data in (b), (d) and (e) is taken from ref. [33,36,38–43].

**Table 1**Dielectric properties and physical constants obtained from Curie-Weiss analysis.

Samples	ε'	tanδ	<i>C</i> '	Tc	T <sub>O-T</sub>	θ <sub>C</sub>
	[-]	[%]	[×10 <sup>5</sup> ºC]	[ºC]	[ºC]	[ºC]
BT-75 nm	690	3.5	1.4	121 ± 1	34 ± 3	27 ± 1
BT-150 nm	1830	4.3	2.7	122 ± 1	38 ± 4	61 ± 1

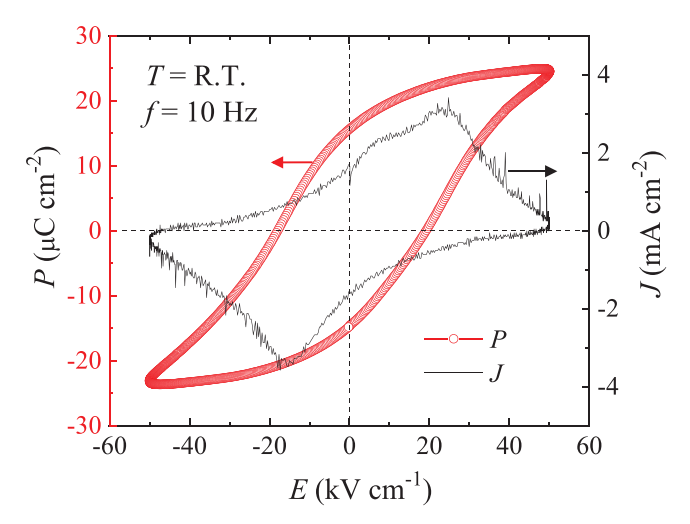


Fig. 4. P-E hysteresis loop of BT-75 nm.

previously thought, recent studies indicate the nanostructure could enhance the ferroelectric properties [51,52]. The understanding of the structure-property relationship in the BaTiO<sub>3</sub> nanocrystalline ceramics is under further investigation and is beyond the scope of this report.

#### 4. Conclusions

In summary, we have successfully densified  $BaTiO_3$  ceramics at 300  $^{\circ}C$  without any secondary heat treatment with the cold sintering

technique. The resulting dielectric permittivity is 700–1800 depending on processing conditions. The dielectric properties are comparable to the reported values considering the grain size effect. The dielectric properties are comparable to the highest quality reported data that required preparation by high temperature sintering techniques (> 1000 °C) reported previously. The sintering temperature in this work is even lower than the processing temperature for high quality  $\rm BaTiO_3$  thin films. The Cold-Sintered  $\rm BaTiO_3$  ceramic shows a  $\it P-E$  loop with relatively high remanent polarization. This work should open up the possibility to densify more inorganic materials at low temperatures in a single step.

### **Declaration of Competing Interest**

There are no conflicts to declare

#### Acknowledgement

Authors would like to acknowledge the late Amanda Baker for her experimental help at the early stage of this project. Authors also would like to thank Ms. Joanne Aller for her help to prepare the manuscript. K.T. is also thankful to Mr. SunHwi Bang for a proper temperature measurement. This material is based upon work supported in part by the National Science Foundation, as part of the Center for Dielectrics and Piezoelectrics under Grant Nos. IIP-1361571 and 1361503. We also thank the members of the many companies that continue to offer support and ideas to drive this work.

## Appendix A. Supplementary data

Supplementary material related to this article can be found, in the online version, at doi:https://doi.org/10.1016/j.jeurceramsoc.2019.12.

### References

 H. Kähäri, M. Teirikangas, J. Juuti, H. Jantunen, Dielectric properties of Lithium molybdate ceramic fabricated at room temperature, J. Am. Ceram. Soc. 97 (2014)

- 3378-3379, https://doi.org/10.1111/jace.13277.
- [2] J. Guo, H. Guo, A.L. Baker, M.T. Lanagan, E.R. Kupp, G.L. Messing, C.A. Randall, Cold Sintering: A Paradigm Shift for Processing and Integration of Ceramics, Angew. Chemie - Int. Ed. 55 (2016) 11457–11461, https://doi.org/10.1002/anie. 201605443.
- [3] J.-P. Maria, X. Kang, R.D. Floyd, E.C. Dickey, H. Guo, J. Guo, A. Baker, S. Funihashi, C.A. Randall, Cold sintering: current status and prospects, J. Mater. Res. 32 (2017) 3205–3218, https://doi.org/10.1557/jmr.2017.262.
- [4] J. Guo, R. Floyd, S. Lowum, J. Maria, T. Herisson de Beauvoir, J. Seo, C.A. Randall, Cold sintering: progress, challenges, and future opportunities, Annu. Rev. Mater. Res. 49 (2019) 275–295, https://doi.org/10.1146/annurev-matsci-070218-010041.
- [5] H. Guo, J. Guo, A. Baker, C.A. Randall, Hydrothermal assisted cold sintering process: a new guidance for low temperature ceramic sintering, ACS Appl. Mater. Interfaces 8 (2016) 20909–20915, https://doi.org/10.1021/acsami.6b07481.
- [6] D. Wang, H. Guo, C.S. Morandi, C.A. Randall, S. Trolier-McKinstry, Cold sintering and electrical characterization of lead zirconate titanate piezoelectric ceramics, APL Mater. 6 (2018) 016101, https://doi.org/10.1063/1.5004420.
- [7] R. Boston, J. Guo, S. Funahashi, A.L. Baker, I.M. Reaney, C.A. Randall, Reactive intermediate phase cold sintering in strontium titanate, RSC Adv. 8 (2018) 20372–20378, https://doi.org/10.1039/C8RA03072C.
- [8] D. Elwell, H.J. Scheel, Crystal Growth from High-Temperature, Academic Press, London, 1975.
- W.K. Ham, G.F. Holland, A.M. Stacy, Low-temperature synthesis of superconducting La<sub>2-x</sub>M<sub>x</sub>CuO<sub>4</sub>: direct precipitation from NaOH/KOH melts, J. Am. Chem. Soc. 110 (1988) 5214–5215, https://doi.org/10.1021/ja00223a063.
- [10] T.L. Friedman, A.M. Stacy, Electrochemistry in molten hydroxides: synthesis of NaCuO<sub>2</sub>, J. Solid State Chem. 109 (1994) 203–204, https://doi.org/10.1006/jssc. 1994.1092.
- [11] S.L. Stoll, A.M. Stacy, C.C. Torardi, Single-Crystal Growth, Alkali Metal Ordering, and Superconductivity in  $\text{La}_{2,x}\text{M}_x\text{CuO}_4(\text{M}=\text{Na},\text{K})$ , Inorg. Chem. 33 (1994) 2761–2765, https://doi.org/10.1021/ic00091a016.
- [12] D. Sandford, L.N. Marquez, A.M. Stacy, Precipitation of superconducting, single phase EuBa<sub>2</sub>Cu<sub>4</sub>O<sub>8</sub> from molten hydroxide at 475 °C, Appl. Phys. Lett. 67 (1995) 422–423, https://doi.org/10.1063/1.114619.
- [13] H. Liu, C. Hu, Z.L. Wang, Composite-hydroxide-mediated approach for the synthesis of nanostructures of complex functional-oxides, Nano Lett. 6 (2006) 1535–1540, https://doi.org/10.1021/pl061253e.
- [14] R.D. Floyd, S.M. Lowum, J.-P. Maria, HYDROFLUX-ASSISTED DENSIFICATION, US Provisional Patent Application. (2019).
- [15] H. Guo, A. Baker, J. Guo, C.A. Randall, Cold sintering process: a novel technique for low-temperature ceramic processing of ferroelectrics, J. Am. Ceram. Soc. 99 (2016) 3489–3507, https://doi.org/10.1111/jace.14554.
- [16] S.H. Bang, A. Ndayishimiye, C.A. Randall, Mechanistic Approach to Identify Densification Kinetics and Mechanisms of Zinc Oxide Cold Sintering, Available SSRN https://Ssrn.Com/Abstract = 3428070 (2019).
- [17] ASTM E112-13, ASTM E112-13: Standard test methods for determining average grain size, ASTM Int. (2013) 1–28, https://doi.org/10.1520/E0112-13.1.4.
- [18] J.P. Gratier, R. Guiguet, Experimental pressure solution-deposition on quartz grains: the crucial effect of the nature of the fluid. J. Struct. Geol. 8 (1986) 856.
- [19] F. Bouville, A.R. Studart, Geologically-inspired strong bulk ceramics made with water at room temperature, Nat. Commun. 8 (2017) 14655, https://doi.org/10. 1038/ncomms14655
- [20] G. Goglio, A. Ndayishimiye, A. Largeteau, C. Elissalde, View point on hydrothermal sintering: main features, today's recent advances and tomorrow's promises, Scr. Mater. 158 (2019) 146–152, https://doi.org/10.1016/j.scriptamat.2018.08.038.
- [21] A. Ndayishimiye, M.Y. Sengul, S.H. Bang, K. Tsuji, K. Takashima, T. Hérisson, D. Beauvoir, D. Denux, J. Thibaud, A.C.T. Van Duin, C. Elissalde, G. Goglio, C.A. Randall, Comparing hydrothermal sintering and cold sintering process: mechanisms, microstructure, kinetics and chemistry, J. Eur. Ceram. Soc. (2019), https://doi.org/10.1016/j.jeurceramsoc.2019.11.049.
- [22] D. Hennings, S. Schreinemacher, Characterization of hydrothermal barium titanate, J. Eur. Ceram. Soc. 9 (1992) 41–46, https://doi.org/10.1016/0955-2219(92) 00075 0
- [23] S. Wada, T. Suzuki, T. Noma, Role of lattice defects in the size effect of barium titanate fine particles, J. Ceram. Soc. Japan. 104 (1996) 383–392, https://doi.org/ 10.2109/jcersj.104.383.
- [24] Y.V. Kolen'ko, K.A. Kovnir, I.S. Neira, T. Taniguchi, T. Ishigaki, T. Watanabe, N. Sakamoto, M. Yoshimura, A novel, controlled, and high-yield solvothermal drying route to nanosized barium titanate powders, J. Phys. Chem. C. 111 (2007) 7306–7318, https://doi.org/10.1021/jp0678103.
- [25] G. Dale, M. Strawhorne, D.C. Sinclair, J.S. Dean, Finite element modeling on the effect of intra-granular porosity on the dielectric properties of BaTiO<sub>3</sub> MLCCs, J. Am. Ceram. Soc. 101 (2018) 1211–1220, https://doi.org/10.1111/jace.15261.
- [26] P. Bendale, S. Venigalla, J.R. Ambrose, E.D. Verink, J.H. Adair, Preparation of barium titanate films at 55 °C by an electrochemical method, J. Am. Ceram. Soc. 76 (1993) 2619–2627.
- [27] J.O. Eckert, C.C. Hung-Houston, B.L. Gersten, M.M. Lencka, R.E. Riman, Kinetics and mechanisms of hydrothermal synthesis of barium titanate, J. Am. Ceram. Soc. 79 (1996) 2929–2939, https://doi.org/10.1111/j.1151-2916.1996.tb08728.x.
- [28] M. Frey, D. Payne, Grain-size effect on structure and phase transformations for

- barium titanate, Phys. Rev. B 54 (1996) 3158–3168, https://doi.org/10.1103/
- [29] U.D. Venkateswaran, V.M. Naik, R. Naik, High-pressure raman studies of polycrystalline BaTiO<sub>3</sub>, Phys. Rev. B 58 (1998) 14256–14260, https://doi.org/10.1103/ PhysRevB.58.14256.
- [30] Y. Shiratori, C. Pithan, J. Dornseiffer, R. Waser, Raman scattering studies on nanocrystalline BaTiO<sub>3</sub> Part II—consolidated polycrystalline ceramics, J. Raman Spectrosc. 9 (2007) 357–364, https://doi.org/10.1002/jrs.
- [31] V. Buscaglia, M.T. Buscaglia, M. Viviani, L. Mitoseriu, P. Nanni, V. Trefiletti, P. Piaggio, I. Gregora, T. Ostapchuk, J. Pokorný, J. Petzelt, Grain size and grain boundary-related effects on the properties of nanocrystalline barium titanate ceramics, J. Eur. Ceram. Soc. 26 (2006) 2889–2898, https://doi.org/10.1016/j. jeurceramsoc.2006.02.005.
- [32] Z. Gui, A. Kang, L. Li, H. Wen, X. Wang, X. Deng, Phase Transitions in Nanocrystalline Barium Titanate Ceramics Prepared by Spark Plasma Sintering, J. Am. Ceram. Soc. 89 (2006) 1059–1064, https://doi.org/10.1111/j.1551-2916. 2005.0836.x.
- [33] G. Arlt, D. Hennings, G. De With, Dielectric properties of fine-grained barium titanate ceramics, J. Appl. Phys. 58 (1985) 1619–1625, https://doi.org/10.1063/1. 336051
- [34] J. Zhu, W. Han, H. Zhang, Z. Yuan, X. Wang, L. Li, C. Jin, Phase coexistence evolution of nano BaTiO<sub>3</sub> as function of particle sizes and temperatures, J. Appl. Phys. 112 (2012) 064110, https://doi.org/10.1063/1.4751332.
- [35] L. Mitoseriu, L.P. Curecheriu, Ceramics: intrinsic versus extrinsic size effects, Nanoscale Ferroelectr. Multiferroics Key Process. Charact. Issues, Nanoscale Eff., 2016, pp. 473–511.
- [36] Z. Zhao, V. Buscaglia, M. Viviani, M.T. Buscaglia, L. Mitoseriu, A. Testino, M. Nygren, M. Johnsson, P. Nanni, Grain-size effects on the ferroelectric behavior of dense nanocrystalline BaTiO3 ceramics, Phys. Rev. B - Condens. Matter Mater. Phys. 70 (2004) 1–8, https://doi.org/10.1103/PhysRevB.70.024107.
- [37] M.T. Buscaglia, V. Buscaglia, M. Viviani, J. Petzelt, M. Savinov, L. Mitoseriu, A. Testino, P. Nanni, C. Harnagea, Z. Zhao, M. Nygren, Ferroelectric properties of dense nanocrystalline BaTiO3 ceramics, Nanotechnology 15 (2004) 1113–1117, https://doi.org/10.1088/0957-4484/15/9/001.
- [38] M.H. Frey, Z. Xu, P. Han, D.A. Payne, The role of interfaces on an apparent grain size effect on the dielectric properties for ferroelectric barium titanate ceramics, Ferroelectrics 206 (1998) 337–353, https://doi.org/10.1080/ 00150199808009168.
- [39] K. Kinoshita, A. Yamaji, Grain-size effects on dielectric properties in barium titanate ceramics, J. Appl. Phys. 47 (1976) 371–373, https://doi.org/10.1063/1.322330.
- [40] A.V. Polotai, A.V. Ragulya, C.A. Randall, Preparation and size effect in pure nanocrystalline barium titanate ceramics, Ferroelectrics 288 (2003) 93–102, https:// doi.org/10.1080/00150190390211972.
- [41] M. Tanaka, Y. Makino, Finite size effects in submicron barium titanate particles, Ferroelectr. Lett. Sect. 24 (1998) 13–23, https://doi.org/10.1080/ 07315179808204451.
- [42] C.A. Randall, D.E. Mccauley, D.P. Cann, Finite size effects in a BaTiO<sub>3</sub> ferroelectric glass ceramic, Ferroelectrics 206 (2007) 325–335, https://doi.org/10.1080/ 00150199808009167.
- [43] Y. Huan, X. Wang, J. Fang, L. Li, Grain size effect on piezoelectric and ferroelectric properties of BaTiO3 ceramics, J. Eur. Ceram. Soc. 34 (2014) 1445–1448, https://doi.org/10.1016/j.jeurceramsoc.2013.11.030.
- [44] S. Roberts, Dielectric constants and polarizabilities of ions, Phys. Rev. 105 (1949) 1215.
- [45] C.J. Johnson, Some dielectric and electro-optic properties of BaTiO $_3$  single crystals, Appl. Phys. Lett. 7 (1965) 221–223, https://doi.org/10.1063/1.1754387.
- [46] D.R. Tilley, B. Žekš, Landau theory of phase transitions in thick films, Solid State Commun. 49 (1984) 823–828, https://doi.org/10.1016/0038-1098(84)90089-9.
- [47] C.A. Randall, Scientific and engineering issues of the state-of-the-art and future multilayer capacitors, J. Ceram. Soc. Japan. 109 (2001) \$2-\$6, https://doi.org/10.
- [48] J.F. Ihlefeld, D.T. Harris, R. Keech, J.L. Jones, J.P. Maria, S. Trolier-McKinstry, Scaling effects in perovskite ferroelectrics: fundamental limits and process-structure-Property relations, J. Am. Ceram. Soc. 99 (2016) 2537–2557, https://doi.org/ 10.1111/jace.14387.
- [49] M.T. Buscaglia, M. Viviani, V. Buscaglia, L. Mitoseriu, A. Testino, P. Nanni, Z. Zhao, M. Nygren, C. Harnagea, D. Piazza, C. Galassi, High dielectric constant and frozen macroscopic polarization in dense nanocrystalline BaTiO<sub>3</sub> ceramics, Phys. Rev. B Condens. Matter Mater. Phys. 73 (2006) 1–10, https://doi.org/10.1103/PhysRevB. 73.064114.
- [50] X. Deng, X. Wang, H. Wen, L. Chen, L. Chen, L. Li, Ferroelectric properties of nanocrystalline barium titanate ceramics, Appl. Phys. Lett. 88 (2006) 1–4, https://doi. org/10.1063/1.2213508.
- [51] Z. Shen, H. Yan, D. Grüner, L.M. Belova, Y. Sakamoto, J. Hu, C.W. Nan, T. Höche, M.J. Reece, Ferroelectric ceramics with enhanced remnant polarization by ordered coalescence of nano-crystals, J. Mater. Chem. 22 (2012) 23547–23552, https://doi. org/10.1039/c2jm32191b.
- [52] M.B. Smith, K. Page, T. Siegrist, A. Et, Crystal structure and the paraelectric-to-ferroelectric phase transition of nanoscale BaTiO<sub>3</sub>, J. Am. Chem. Soc. 130 (2008) 6955–6963.